

Impact of land–sea thermal contrast on interdecadal variation in circulation and blocking

Yongli He · Jianping Huang · Mingxia Ji

Received: 4 October 2013 / Accepted: 27 February 2014
© The Author(s) 2014. This article is published with open access at Springerlink.com

Abstract The impact of asymmetric thermal forcing associated with land–sea distribution on interdecadal variation in large-scale circulation and blocking was investigated using observations and the coupled model intercomparison project outputs. A land–sea index (LSI) was defined to measure asymmetric zonal thermal forcing; the index changed from a negative to a positive anomaly in the 1980s. In the positive phase of the LSI, the 500 hPa geopotential height decreased in the polar regions and increased in the mid-latitudes. The tropospheric planetary wave activity also became weaker and exerted less easterly forcing on the westerly wind. These circulation changes were favorable for westerly wind acceleration and reduced blocking. In the Atlantic, the duration of blocking decreased by 38 % during the positive LSI phase compared with that during the negative phase; in Europe, the number of blocking persisting for longer than 10 days during the positive LSI phase was only half of the number during the negative phase. The observed surface air temperature anomaly followed a distinctive “cold ocean/warm land” (COWL) pattern, which provided an environment that reduced, or destroyed, the resonance forcing of topography and was unfavorable for the development and persistence of blocking. In turn, the responses of the westerly and blocking could further enhance continental warming, which would strengthen the “cold ocean/warm land” pattern. This positive feedback amplified regional warming in the context of overall global warming.

Keywords Land–sea thermal contrast · Atmospheric circulation · Blocking · Cold ocean/warm land pattern

1 Introduction

Under global warming, the warming of surface air temperature (SAT) became much more enhanced during cold season than during warm season in the second half of the twentieth century (Manabe and Stouffer 1980; Robock 1983; Folland et al. 1990; Jones and Briffa 1992; Huang et al. 2012). The boreal winter warming trend is the highest in semi-arid regions with an increase of 1.53 °C and contributed to 44.46 % of the global annual-mean land surface temperature increase (Huang et al. 2012, 2013). In the Northern Hemisphere an apparent flattening in the trend since 1998 was noted by Cohen et al. (2012), but the data is too short to discuss this most recent change in the trend.

The global temperature change during the second half of the 20th century is closely related to changes in atmospheric circulation during winter. Gong and Wang (1999) investigated changes in the intensity of the Siberian high based on a monthly-mean sea level pressure (SLP) data set for the Northern Hemisphere obtained from the Climate Research Unit (CRU) at the University of East Anglia in the UK. He found that the Siberian high had weakened in recent decades, which led to weakened cold surges from the Arctic in the East Asia in winter. Wang et al. (2009) investigated the interannual variation of the East Asian Trough (EAT) axis at 500 hPa and determined that both the trough intensity index and trough axis index had linear downward trends. When the tilt of the EAT was smaller than normal, the East Asian winter monsoon tended to take a southern pathway, and less cold air moved to the central North Pacific. During the positive phase of the North

Y. He · J. Huang (✉) · M. Ji
Key Laboratory for Semi-Arid Climate Change of the Ministry of Education, College of Atmospheric Sciences, Lanzhou University, Lanzhou 730000, China
e-mail: hjp@lzu.edu.cn

Atlantic Oscillation (NAO), the blocking in the North Atlantic consistently tended to decrease and weaken (Shabbar et al. 2001; Luo 2005; Huang et al. 2006; Ji et al. 2008). Therefore, during the last few decades of the twentieth century, a significant winter warming trend was usually accompanied by weakened cold surge. Attention was, however, focused on the influence of sea surface temperature (SST); for example, the North Atlantic SST can modulate the phase of the interdecadal component of the NAO (Higuchi et al. 1999; Kucharski et al. 2005); the correlation between El Niño/Southern Oscillation (ENSO) and Asian monsoon is apparent in the wavelet cross-spectrum (Hudgins and Huang 1996; Huang et al. 1998). Few studies investigated the responses of atmospheric circulation to land temperature changes, although the land surface temperature is more sensitive to climate change. Studies are also needed to determine whether feedback exists between the temperature change in the underlying surface and the circulation anomaly above.

Many studies have shown a strong relationship between blocking activity in the Northern Hemisphere and zonal mean flow (Egger 1978; Charney and DeVore 1979; Tung and Lindzen 1979; Kaas and Branstator 1993). They suggested that the formation and development of blocking can be explained by the linear resonance of planetary waves with surface thermal forcing and topographical forcing. Shabbar et al. (2001) found that blocking frequency and persistence are sensitive to the phase of the NAO. In the positive phase of the NAO, the distribution of the SAT anomaly follows the “cold ocean/warm land” (COWL) pattern, which reduces, or destroys, the resonance forcing of topography. Although the thermal forcing pattern over the Northern Hemisphere has been shown to be relatively consistent with this theory, much less effort has been devoted to a dynamical explanation of the enhanced warming in the boreal winter. Therefore, the first goal of this study is to understand the relationship between land–sea thermal contrast and interdecadal variation in large-scale circulation, using the theory based on a simplified low-order theoretical model of Charney and DeVore (1979). The second goal is to identify any feedback between COWL pattern and the responses of the circulation.

The paper is arranged as follows. Section 2 describes the data sources. In Sect. 3, we define the land–sea index (LSI) used to measure the changes in the land–sea thermal contrast associated with the enhanced warming in cold season. Section 4 provides a brief description of the responses of atmospheric circulation to the change in thermal forcing. Section 5 discusses the relationship between blocking frequency and the land–sea thermal contrast. Verification of the feedback between COWL pattern and the responses of the circulation is made using the coupled model

intercomparison project (CMIP5) data sets in Sect. 6. A summary and discussion are provided in Sect. 7.

2 Data and methods

The data set used in this study includes the daily geopotential height (GPH) and wind fields and monthly wind field of the NCEP-NCAR reanalysis from the Climate Diagnostics Center of the National Oceanic and Atmosphere Administration (NOAA). The resolution is $2.5^\circ \times 2.5^\circ$ horizontally with 17 levels in the vertical direction (Kalnay et al. 1996). It covers the time period from January 1948 to May 2012. We use December–February (DJF) mean for winter (or cold season). The monthly-mean SAT was obtained from the CRU, version TS3.2 (Mitchell and Jones 2005). It covers the period of 1901–2011 and has a horizontal resolution of $0.5^\circ \times 0.5^\circ$. The time series of monthly-mean SST is provided by the Hadley Center for Climate Prediction and Research of the UK Met Office and covers the period of 1870 to the present at a spatial resolution of $1.0^\circ \times 1.0^\circ$ (Rayner et al. 2003). The Arctic Oscillation (AO) time series was obtained from the website (<http://ljp.lasg.ac.cn/dct/page/65569>); the AO is defined as the difference of the normalized monthly zonal-mean SLP between 35°N and 65°N .

3 The land–sea index

To investigate the impact of land–sea thermal contrast on enhanced warming in the cold season in the Northern Hemisphere, we focus on winter when the land–sea thermal contrast is the largest.

3.1 The COWL pattern

First, we present the anomaly patterns associated with low-frequency variability in the Northern Hemisphere extratropics. Figure 1 shows the second empirical orthogonal function (EOF) associated with the second principal component of 500 hPa GPH anomalies over the extratropics (20° – 80°N), which explains 16 % of the total variance. This pattern has been discussed by many authors (e.g., Wallace et al. 1996; Wu and Straus 2004, hereafter as WS04), with broadly consistent results. Wallace et al. (1996) named the pattern the “cold ocean–warm land” (COWL) pattern, which accounts for 65 % of the SAT variance during the cold season. They pointed out that the anomalous warming in the winters of the 1980s was consistent with a strong positive bias of the COWL pattern index. WS04 compared the pattern using traditional and modified COWL definitions; the latter was defined using

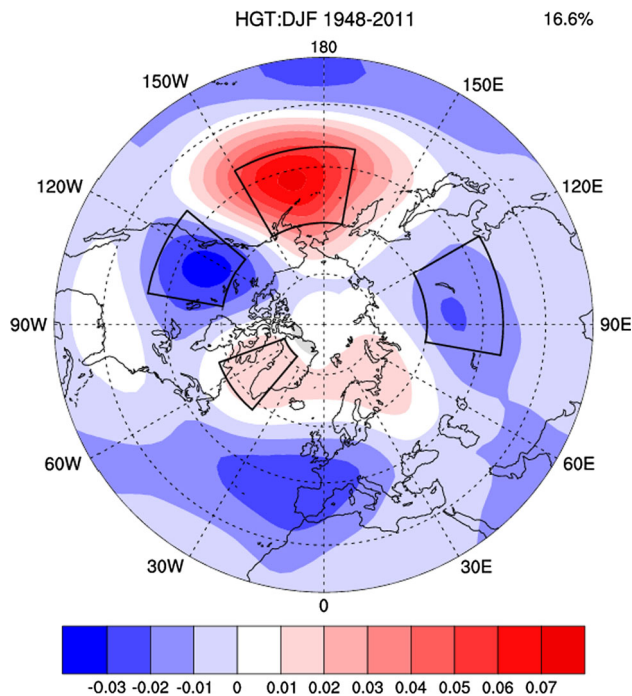


Fig. 1 The second EOF of December–February mean 500 hPa GPH during 1948–2011, in the Northern Hemisphere domain of 20°–80°N

the second EOF of 500 hPa GPH. They found that the mid-tropospheric temperature trend was mostly due to the COWL pattern, with the AO representing only the local cooling over Greenland.

3.2 The land–sea index

Since the surface thermal pattern can influence the alternation of two possible dynamic equilibria (wave-like or zonal component), it is crucial to quantify the intensity of the asymmetric thermal forcing. Molteni et al. (2011) defined it as the zonal wave-2 component of the net surface heat flux averaged in four sectors of 90° longitude each. Although this definition can represent the land–sea thermal contrast, it does not correspond to the region of maximum land–sea contrast. From Fig. 1, we can clearly identify a wave-2 distribution from the “COWL” pattern induced by the land–sea distribution. We select four pattern centers as key areas.

$$\begin{aligned} \text{LSI} = & T_{\text{ano}}[80^{\circ}\text{--}120^{\circ}\text{E}, 40^{\circ}\text{--}60^{\circ}\text{N}] - T_{\text{ano}} \\ & \times [170^{\circ}\text{E}\text{--}150^{\circ}\text{W}, 40^{\circ}\text{--}60^{\circ}\text{N}] \\ & + T_{\text{ano}}[130^{\circ}\text{--}100^{\circ}\text{W}, 40^{\circ}\text{--}60^{\circ}\text{N}] \\ & - T_{\text{ano}}[70^{\circ}\text{--}40^{\circ}\text{W}, 57.5^{\circ}\text{--}77.5^{\circ}\text{N}], \end{aligned}$$

where T_{ano} is an area-averaged surface temperature anomaly with respect to the period of 1960–1990.

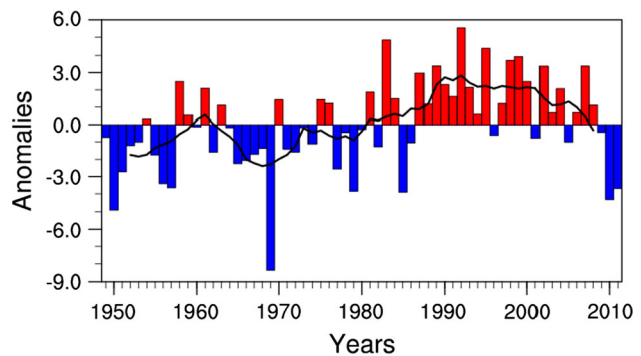


Fig. 2 Time series of land–sea index in winter, the *black curve* indicate 7-year Gaussian-type filtered values

Unlike the Molteni’s COWL index, which is based on a regular wave structure explicitly, we define it as a linear combination of the average surface temperature anomaly in the key areas of the COWL pattern, to eliminate the temperature difference between different latitudes. Since the latent heat is close to zero in winter, we only need to consider sensible heat difference between land and ocean. Since the LSI defined by net surface heat flux in the four key areas is similar to that defined by the temperature anomaly, we choose the LSI defined by temperature anomaly to represent the land–sea thermal contrast for simplicity. Because the heat capacity of the land is much smaller than that of the ocean, the warming on a continent in winter is much stronger than that over the ocean under global warming. Therefore, the positive LSI indicates a warmer climate and smaller land–sea temperature difference. The LSI changes from a negative to a positive phase, which represents a decrease in the land–sea thermal contrast, in winter due to anomalous warming over the land.

Figure 2 shows the decadal variability of the LSI anomaly in winter. Clearly, in the second half of the twentieth century the LSI was increasing and changed from a negative to a positive anomaly in the 1980s. However, the LSI index displayed a decreasing trend after the 2000s. Consistent with these results, a recent study has found that the largest regional contributor to global temperature trend over the past two decades was SAT in the Northern Hemisphere extra tropics. Rapid and significant warming was evident in all the seasons but winter season; during winter the linear temperature trend was nearly zero. However, corresponding to the near-neutral wintertime trend were large regions of significantly strong cooling trends across Europe, northern and central Asia, and part of central and eastern North America (Cohen et al. 2012). Due to the shortage of data for identification of such short-term trend, we focus on the second half of the twentieth century in this study.

With the enhanced winter warming in Eurasia and North America in the second half of the twentieth century, the

Fig. 3 Composites of 500 hPa geopotential height anomalies in winter (DJF) for (a) positive land–sea index and (b) negative land–sea index. c Difference between positive and negative LSI phases (positive minus negative). The contour intervals are 10 m in (a) and (b), and 20 m in (c). The shaded areas in (c) indicate significant values at the 99 % confidence level

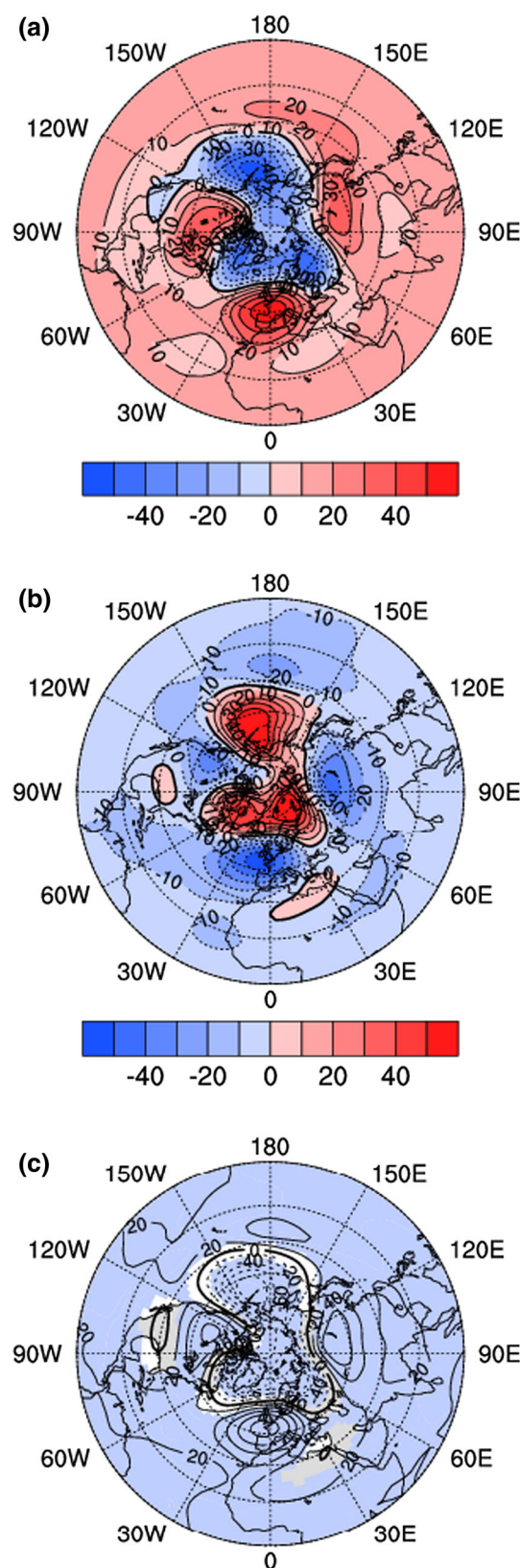
thermal contrast between land and ocean changed its phase since the 1980s (Fig. 2). Following Charney-DeVore's equilibrium theory, when the zonal asymmetric thermal contrast exceeds a certain threshold, the atmospheric circulation would change from one equilibrium to the other. This leads to the question of whether there is a relationship between the land-sea thermal contrast and the COWL pattern. Although the COWL pattern is important for understanding the internal variability of atmospheric circulation, there were few studies on the mechanism of the COWL pattern. As advocated in Kucharski et al. (2005), heat fluxes generated in the North Pacific may induce SST anomalies in the subtropical Pacific on decadal timescale and embed a COWL-like pattern to sustain the NAO through the cooling of the subtropical West Pacific and a consequent enhancement of the west Tropical Pacific SST gradient.

4 Atmosphere circulation associated with LSI

4.1 500 hPa GPH and SLP

The westerly wind index in Fig. 5a is an obvious measure of the intensity of the mid- to high-latitude westerly wind. The index is computed using a modified definition by Li and Wang (2003), namely, the difference in zonal mean SLP between 35°N and 65°N from the monthly NCEP/NCAR reanalysis data, which contains a larger signal-to-noise ratio than the traditional zonal index suggested by Rossby (1939). The anomaly of the westerly wind index changed its sign in the 1980; its correlation coefficient with the LSI was 0.49 and rose to 0.89 after applying a 7-year Gaussian filter. Both coefficients significantly exceed the 99 % confidence level. The result indicates that the westerly wind became stronger, as the LSI changed from a negative to a positive phase.

To investigate the responses of atmospheric circulation to the change in the thermal forcing associated with the land–sea distribution, the 500 hPa GPH anomaly and the SLP anomaly patterns must be considered. Here, a composite analysis is carried out to measure the impact of land–sea thermal forcing on the circulation. In our analysis, we select the positive and negative LSI cases in DJF when the absolute normalized value of the LSI was larger than 1.0. Based on this criterion, the negative LSI cases are 1950,



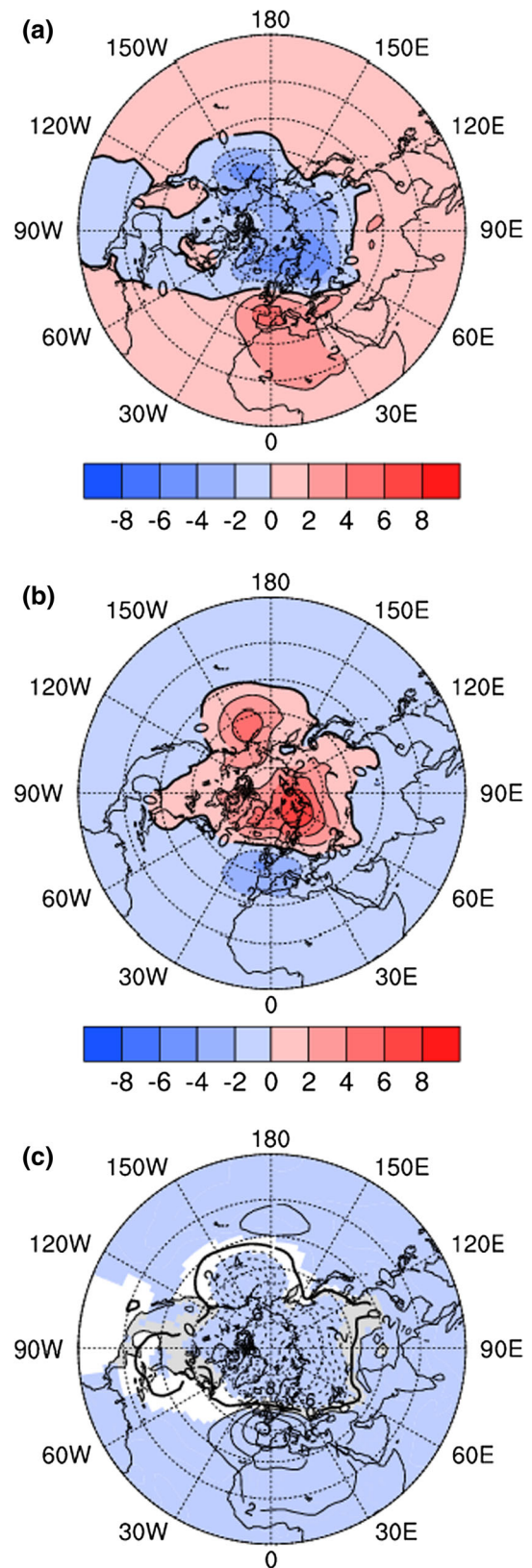
1951, 1956, 1957, 1969, 1979, 1985, 2010, and 2011, and the positive LSI cases are 1983, 1987, 1989, 1992, 1995, 1998, 1999, 2002, and 2007. Figure 3 shows the structures

Fig. 4 Same as Fig. 3, except for SLP anomalies in winter (DJF). ▶ The contour intervals are 1 hPa in (a) and (b) and 2 hPa in (c). The shaded areas in (c) indicate significant values at the 99 % confidence level

of monthly-mean 500 hPa GPH anomaly field for positive LSI phase, negative LSI phase and the difference between the two composites. As with previous studies, the anomaly pattern indicates that in the positive LSI phase, 500 hPa GPH decreased in the Arctic region, with the negative anomaly extending into the North Atlantic and Northwest Pacific, and increased over North America and the Eurasian Continent in the mid-latitudes, which increased the meridional gradient of GPH between mid and high latitudes. As shown by the shaded areas in Fig. 3c, these differences between the positive and negative phases significantly exceed the 99 % confidence level for the two-sided Student's *t* test. To further clarify the difference in 500 hPa GPH, we examined the structures of the monthly-mean SLP anomaly field for positive and negative LSI phases and their difference (Fig. 4). Prominent changes in strength and position are found for semi-permanent pressure centers in different phases of the LSI. The Azores high and the Icelandic low, as captured by the positive- and negative-SLP anomaly centers, were stronger in the positive-LSI (Fig. 4a). Similar to Favre and Gershunov (2006), the Aleutian low was deeper and shifted eastward (shown in Fig. 4c), which advected warmer and moister air masses along the west coast of North America. Consistent with Fig. 3, the Siberian high weakened, with a negative anomaly in the 500 hPa GPH and SLP in the Siberian area (Gong and Wang 1999; Panagiotopoulos et al. 2005). The semi-permanent centers were induced by the land–sea distribution and modulated by planetary waves, so these changes in strength and position may be caused by the increase in the LSI.

4.2 Zonal-mean westerly wind and planetary waves

Chen et al. (2005) pointed out that the quasi-stationary planetary waves may play a role bridging the AO and climate anomalies. The amplitudes of the planetary waves in the lower troposphere over mid-to-high latitudes is affected by the impact of the AO or westerly wind intensity on the vertical propagation of planetary waves. It is of interest to determine whether the spatial pattern of thermal forcing, as external forcing, is related to the magnitude and propagation of planetary waves. To investigate this relationship, we adopt the tropospheric interannual oscillation index (TIO) defined by Chen et al. (2002) to measure the activity of planetary waves. The index is defined as the difference in the Eliassen–Palm (EP) flux divergence of planetary waves between 50°N at 500 hPa and 40°N at



300 hPa. Here, we expand the seasonal-mean GPH into zonal Fourier harmonics and use the sum of the zonal wavenumbers 1–3 to represent the stationary planetary

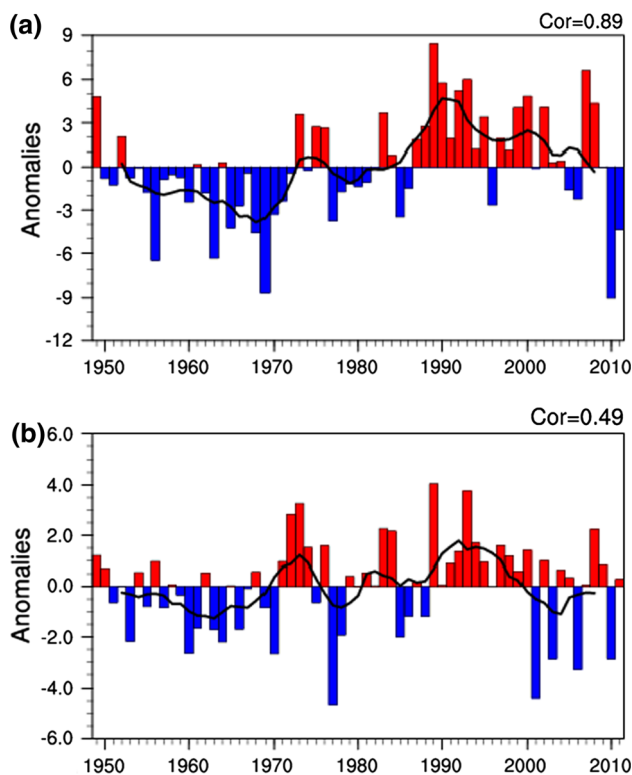


Fig. 5 **a** Winter (DJF) mean time series (1948/1949–2008/2009) of the westerly wind index. The *black curves* indicate 7-year Gaussian-type filtered values. **b** Same as in (a) except for the TIO index

waves. A positive TIO index anomaly indicates larger equatorward propagation of planetary waves and more energy of planetary waves trapped in the troposphere, according to Chen et al. (2002). Figure 5b shows that planetary wave activity in the mid-latitudes became less active in recent decades due to larger equatorward propagation and weaker upward wave refraction into the polar region, and that the correlation coefficient between TIO and LSI is 0.49, exceeding the 99 % confidence level. When the LSI was in a positive phase, equatorward propagation of planetary wave activity also became stronger due to land–sea thermal forcing. Figures 6d–f show the divergence of the zonally averaged EP flux induced by planetary wave activity in latitude–height cross sections for positive phase, negative LSI phase, and the difference between the two composites. In both positive- and negative-phase winters, the EP flux was convergent in most of the extra tropical troposphere, resulting in an easterly wind forcing on the westerly wind exerted by planetary waves. In the difference map, in the mid-latitudes positive values appeared along the polar wave guide and negative values arose along the equator wave guide. The positive values indicate that during winters of positive LSI phase the forcing exerted by planetary wave activity on the westerly wind was weaker than that during winters of negative LSI

phase, which helped to accelerate the westerly wind. The shaded areas in Fig. 6f indicate where the differences between the positive and negative LSI phases significantly exceeded the 95 % confidence level.

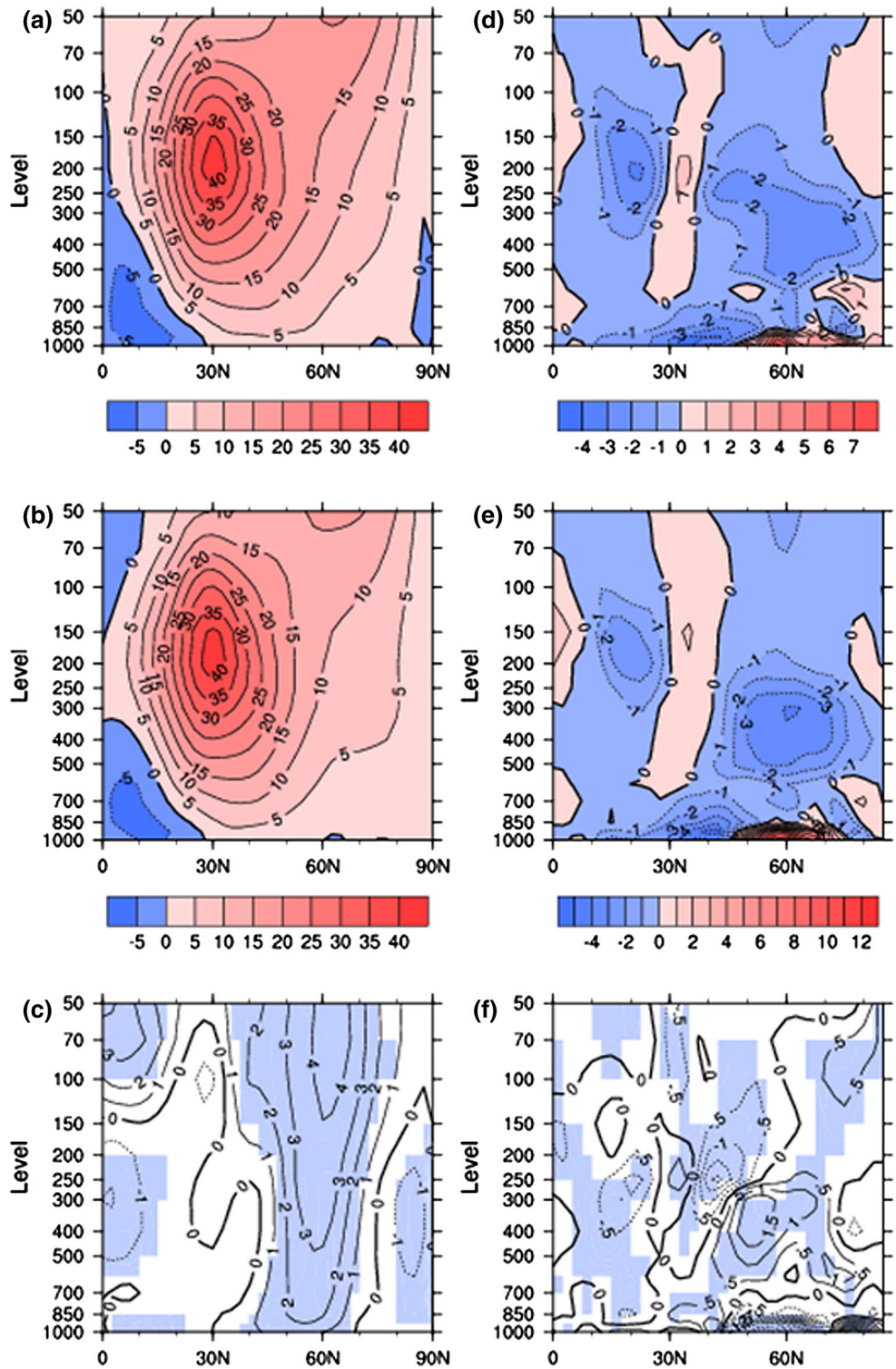
Figure 6a–c shows the composites of zonally-averaged wind for winters with positive and negative LSI phases and the difference between the two phases. The clearly reduced (enhanced) westerly wind appeared around 30°N (60°N), respectively, which resulted in a poleward shift of the subtropical jet stream. This is consistent with previous studies that showed the interannual variability of planetary wave activity was positively correlated with the activity of the westerly wind or the AO (Limpasuvan and Hartmann 1999; Chen et al. 2005). The increasing LSI since the 1980s may be linked to a stronger westerly wind through a larger TIO index. During the winters with larger TIO index, the upward wave propagation from the troposphere into the stratosphere became weaker, and the low-latitude waveguide prevailed, accompanied by an apparently weaker East Asian trough and Siberian high, which are consistent with the observations.

5 Impact of asymmetric thermal contrast on blocking

Blocking is the primary weather system accompanying the invasion of cold air, and induces a wide range of cooling effects. The decrease in Ural blocking contributed to the higher frequency of warm winters in China (Wang et al. 2010). Several theories regarding the formation and maintenance of blocking events have been proposed, including nonlinear interactions between planetary waves or between large-scale flow and transient eddies (Egger 1978; Kung et al. 1990). A number of studies recognized that blocking may be the result of the adjustment of planetary waves to deviations in the zonal-mean flow or the linear resonance of planetary waves with surface forcing (Kaas and Branstator 1993). Recently, a decisive contribution of the NAO to the occurrence of wintertime blocking over the Atlantic sector was proposed by Shabbar et al. (2001), who established a simple conceptual model based on the Charney and DeVore’s theory that blocking is a metastable equilibrium alternating between two equilibrium states of high-index flow (weak wave-like component) and low-index flow (strong wave-like component), which are associated with the NAO phases. Therefore, the NAO can significantly influence the winter SAT by moderating blocking frequency and intensity.

As with many other studies, blocking events were shown to be relatively more frequent over the central Pacific Ocean and the eastern North Atlantic Ocean in cold season, whereas blocking activity was lower over the continents. These results support the existence of four different blocking sectors, as

Fig. 6 *Left panels* composites of globally averaged zonal wind in winter (DJF) for (a) positive LSI phase and (b) negative LSI phase. c The difference between positive and negative LSI phases, i.e. (a) minus (b). The contour intervals are 5 m/s in (a) and (b) and 1 m/s in (c). *Right panels* same as the *left panels*, except for the DJF EP flux divergence induced by planetary waves. The contour interval is 0.50/ms/day and the shaded areas in bottom panels indicate significant values at the 99 % confidence level



shown in Table 1 (Barriopedro et al. 2006). An objective blocking index defined by Tibaldi and Molteni (1990) is used in this study. Here, a brief definition is given in order to facilitate our discussion. The 500 hPa GPH gradients, namely, GHGS and GHGN are computed for each longitude:

$$GHGS = \frac{Z(\phi_0) - Z(\phi_s)}{\phi_0 - \phi_s}$$

$$GHGN = \frac{Z(\phi_n) - Z(\phi_0)}{\phi_n - \phi_0}$$

Table 1 Blocking sectors defined in this study

	Euro-Atlantic		Pacific	
Sector	ATL	EUR	WPA	EPA
Domain	(100°W, 0°)	(0°, 90°E)	(90°E, 180°)	(180°, 100°W)

where $\phi_n = 80^\circ N + \Delta$, $\phi_0 = 60^\circ N + \Delta$, $\phi_s = 40^\circ N + \Delta$ and $\Delta = -2.5^\circ, 0^\circ, 2.5^\circ$. Since the re-analysis data are on a 2.5° grid, we choose the spacing between latitudes to be 2.5° as well. A given longitude is defined as blocked on a specific day if both of the following conditions are met, GHGS >0 , and GHGN ≤ 10 m per degree latitude. The local blocking index is further constrained by imposing additional space and time constraints in order to obtain a regional blocking signature. If a blocking-like pattern existed over three or more adjacent longitudes and lasted for 5 days or longer, it is considered a regional blocking event. The blocked days are obtained by simply counting the number of days considered as blocked (5 days or longer) by the blocking index for December–February.

The blocking days display an apparent interannual and interdecadal variability in the four regions, but only those in Europe and western Pacific significantly decreased, with linear trends of -13% and -4.9% , respectively, at the 99% confidence level. The North Atlantic region exhibited significant interdecadal variation and experienced a climate shift in the mid 1980s, but its averaged blocked days did not decrease. To examine the relationship between the LSI and regional blocking activity, a composite analysis is performed. The parameters of blocking, such as the averaged number of blocked days per winter, duration, and event numbers, are shown in Table 2. The numbers of blocked days in winter during the negative LSI phases were 11.3, 14.1, 5.7, and 2.9 days longer than during the positive LSI phase in the four sectors, respectively. From the linear trend of blocked days, it is also possible to determine that the mechanism controlling the blocking activity was different in the Atlantic compared with that in the Pacific. The average duration of blocking events in the Atlantic region was 10.1 and 11.8 days during the positive and negative phase, respectively. By comparing the number of events of 5–9 days with that of more than 10 days in the Atlantic region, the reduced blocked days in the positive phase than in the negative phase was found to be caused by fewer longer blocking events. However, in the Europe region, the duration of blocking in the two phases did not change much but the total number of blocking events in the negative LSI phase was much bigger than that in the positive LSI phase. For example, the number of blocking events with the duration of 5–9 days in the positive LSI phase was 16, whereas it was 11 in the negative LSI phase; the number of events with the duration >10 days in the positive phase

Table 2 Composite analysis of blocking parameters (columns) for the Northern Hemisphere and blocking sectors (rows) defined in Table 1

	Trend (day/ year)	Mean days (day)		Duration (day)		Event number			
						5–9 days		≥ 10 days	
		Pos	Neg	Pos	Neg	Pos	Neg	Pos	Neg
ATL	0.05	18.1	29.4	10.1	11.8	7	9	10	14
EUR	-0.13	21.6	35.7	9	11.8	16	11	7	15
WPA	-0.049	14.3	20	11.3	11.5	5	14	8	7
EPA	0.02	18.1	21	10.1	9.7	16	13	4	7

was 7, whereas it was 15 in the negative phase. These results show that, in comparison with the negative phase, it was difficult for the blocking to maintain in the positive phase, so that blockings could not last long. Therefore the environment during the negative LSI phase is considered more favorable to the persistence of blocking. In the western and eastern Pacific regions, when the LSI moved from the negative to the positive phase, fewer short-duration blocking events occurred in the western Pacific region; the opposite situation occurred in the eastern Pacific region. Other mechanisms may influence blocking in these regions. As suggested by Molteni et al. (2011) the zonal thermal contrast over the North Atlantic sector is to a large extent responsible for the circulation pattern there and the NAO, while in the Pacific sector the meridional temperature advection may be a primary forcing that modifies the circulation pattern. After the 2000s, the surface temperature has shown an apparent flattening in trend in the Northern Hemisphere winter (Cohen et al. 2012); however, the blocked days in winter have an obvious upward trend only in the Atlantic sector.

6 Verification of the feedback

To verify the feedback between surface thermal contrast and large-scale circulation, we use the outputs from 23 global climate models (Table 3) to undertake a sensitivity analysis. The outputs were obtained from the CMIP5 multi-model data archive (<http://cmip-pcmdi.llnl.gov/cmip5/index.html>). Following the CMIP5 naming conventions, these are preindustrial control simulation (picontrol) and transient 1% per year increase in CO₂ over the simulation period (1pctco2). The picontrol experiment ran for 500 years by imposing non-evolving, pre-industrial conditions and served as the baseline for the analysis of future scenario runs with prescribed concentrations. The 1pctco2 experiment represents a warm climate state under increased greenhouse gas concentrations. The 1pctco2 experiment was initialized from the pre-industrial control and CO₂

Table 3 a list of CMIP5 GCMs used in this study with a brief description. The picontrol run and 1pctco2 run from each model are used. The first ensemble run is used if a model has multiple ensemble runs

	Model name	Resolution (lon by lat)	Origin
1	BCC-CSM1.1	2.815 × 2.815	Beijing Climate Center, China
2	CCSM4	1.25 × 0.9	National Center for Atmospheric Research, USA
3	CESM1-BGC	1.25 × 0.9	National Center for Atmospheric Research, USA
4	CESM1-CAM5	1.25 × 0.9	National Center for Atmospheric Research, USA
5	CMCC-CM	0.75 × 0.75	Centro Euro-Mediterraneo per i Cambiamenti, Italy
6	CNRM-CM5	1.40 × 1.40	Centre National de Recherches Meteorologiques, France
7	CSIRO-Mk3.6	1.875 × 1.875	Commonwealth Scientific and Industrial Research, Australia
8	FGOALS-g2	2.815 × 3.0	Institute of Atmospheric Physics, CAS, China
9	GFDL-CM3	2.5 × 2.0	Geophysical Fluid Dynamics Laboratory, USA
10	GFDL-ESM2G	2.5 × 2.0	Geophysical Fluid Dynamics Laboratory, USA
11	GFDL-ESM2 M	2.5 × 2.0	Geophysical Fluid Dynamics Laboratory, USA
12	GISS-E2-H	2.5 × 2.0	NASA Goddard Institute for Space Studies, USA
13	GISS-E2-R	2.5 × 2.0	NASA Goddard Institute for Space Studies, USA
14	HadGEM2-ES	1.875 × 1.25	Met Office Hadley Centre, UK
15	INM-CM4	2.0 × 1.5	Institute for Numerical Mathematics, Russia
16	IPSL-CM5A-LR	3.75 × 1.875	Institut Pierre-Simon Laplace, France
17	IPSL-CM5A-MR	2.5 × 2.5	Institut Pierre-Simon Laplace, France
18	IPSL-CM5B-LR	3.75 × 3.75	Institut Pierre-Simon Laplace, France
19	MIROC5	1.40 × 1.40	Atmosphere and Ocean Research Institute, Japan
20	MIROC-ESM	2.815 × 2.815	Japan Agency for Marine-Earth Science and Technology, Japan
21	MPI-ESM-LR	1.875 × 1.875	Max Planck Institute for Meteorology, Germany
22	MRI-CGCM3	1.125 × 1.125	Meteorological Research Institute, Japan
23	NorESM1-M	2.5 × 1.875	Norwegian Climate Centre, Norway

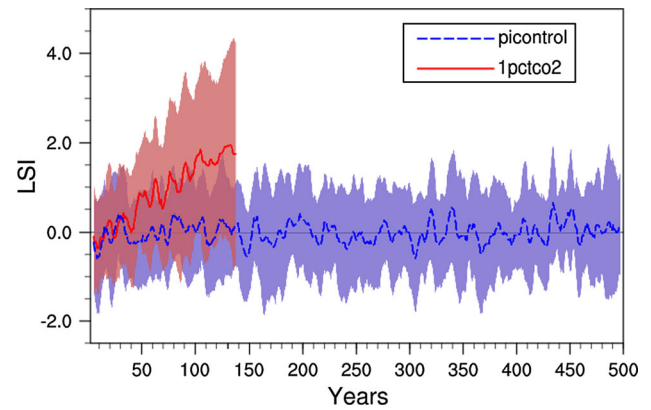


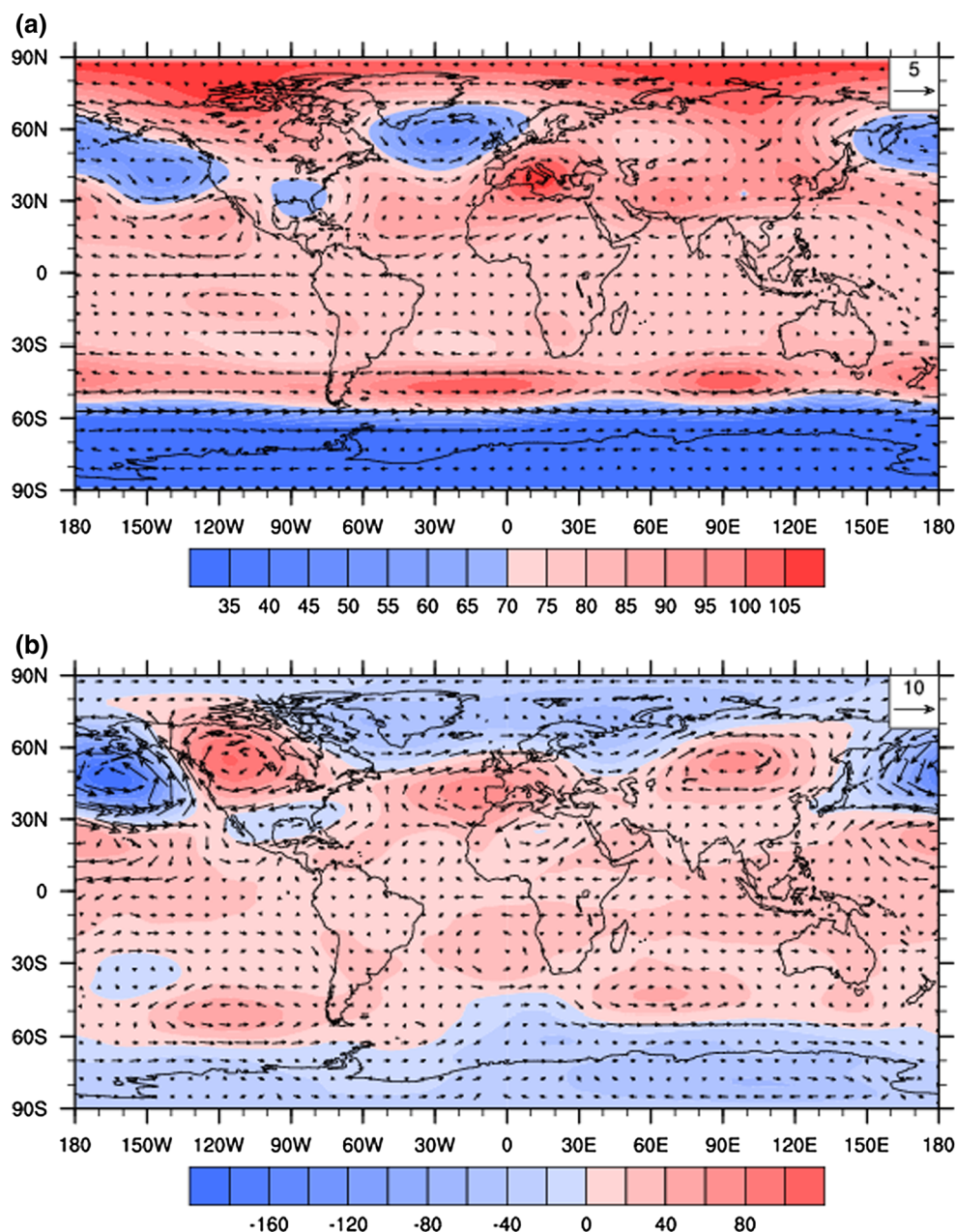
Fig. 7 Time series of the LSI in the 1pctco2 and picontrol experiments. The *red solid curve* represents the ensembles mean of the 1pctco2 experiment, and the *blue dashed curve* represents the ensembles mean of the picontrol experiment. The *shading* denotes one standard deviation of the 23 models from the picontrol/1pctco2 simulations. A 7-year running smoothing was applied to emphasize the climate change

concentration was prescribed to increase at 1 % per year for 140 years (reaching $4 \times$ pre-industrial levels at the end). The boundary conditions for each experiment were described in Taylor et al. (2012).

Figure 7 shows in the picontrol run the LSI oscillated around zero, but in the 1pctco2 run the LSI gradually increased along with increasing CO_2 concentration and a general warming at the global scale. We consider that in the picontrol run the CO_2 concentration was low and the LSI also oscillated around the climate mean state. When the LSI increased and was accompanied by global warming, the system departed from the climate mean state and was in the positive anomaly, which triggered the positive feedback mechanism. At that point, the large-scale circulation shifted from one equilibrium (wave component) to the other (zonal component). As mentioned earlier, the changes in atmospheric circulation and the LSI would form a positive feedback, and the mechanism accelerated the warming process.

To verify the response of large-scale circulation to the change of the LSI, we compare the two experiments during the years 100–140 based on the ensemble average of the 23 models. Here the picontrol experiment represents a low LSI scenario and the 1pctco2 experiment represents a high LSI scenario. Figure 8 shows the differences in GPH and wind fields between the positive and negative LSI phases in the experiments (Fig. 8a) and NCEP (Fig. 8b). In Fig. 8b, the change of GPH in the COWL pattern is very clear in Northern Hemisphere, with higher GPHs over two continents and lower GPHs over two oceans. Due to the CO_2 concentration being quadrupled in the 1pctco2 experiment, the level of global warming is more intense than would be otherwise. Although the 500 hPa GPH increased globally,

Fig. 8 **a** Differences of geopotential height and wind fields between the 1pctco2 and picontrl experiments during years 100–140 based on the ensemble average of the 23 models; **(b)** Same as **(a)**, except using the NCEP data between the positive and negative phase of the COWL index



the pattern highlighting the differences in the oceans—land contrast between the 1pctco2 and picontrl (Fig. 8a) is similar to the reanalysis (Fig. 8b), even though the magnitude of change is smaller in the former than that in the later. Because other forcing factors such as the ENSO, the NAO or polar vortex have changed and interacted under the increasing CO₂ concentration scenario (Huang et al. 1998, 2006), maybe an additional sensitivity experiment is needed, in which the other forcing factors are prescribed.

The composite analysis in Sects. 4 and 5 shows that when the LSI was in the positive phase, the westerly wind was stronger and less blocking activity occurred. The large-

scale circulation change results in a heat advection pattern that enhances the COWL pattern. To verify this, we calculate the temperature advection between different phases of the COWL index and their difference based on NCEP reanalysis data as shown in Fig. 9. Figure 9 shows that the temperature advection was mainly distributed at the junction of continents and oceans and in Eurasian inland areas. As seen from the different fields, the warm advection over eastern part of continents and cold advection over western part of oceans in the positive phase of the COWL index were stronger than those in the negative phase, which is consistent with the results in Sects. 4 and 5.

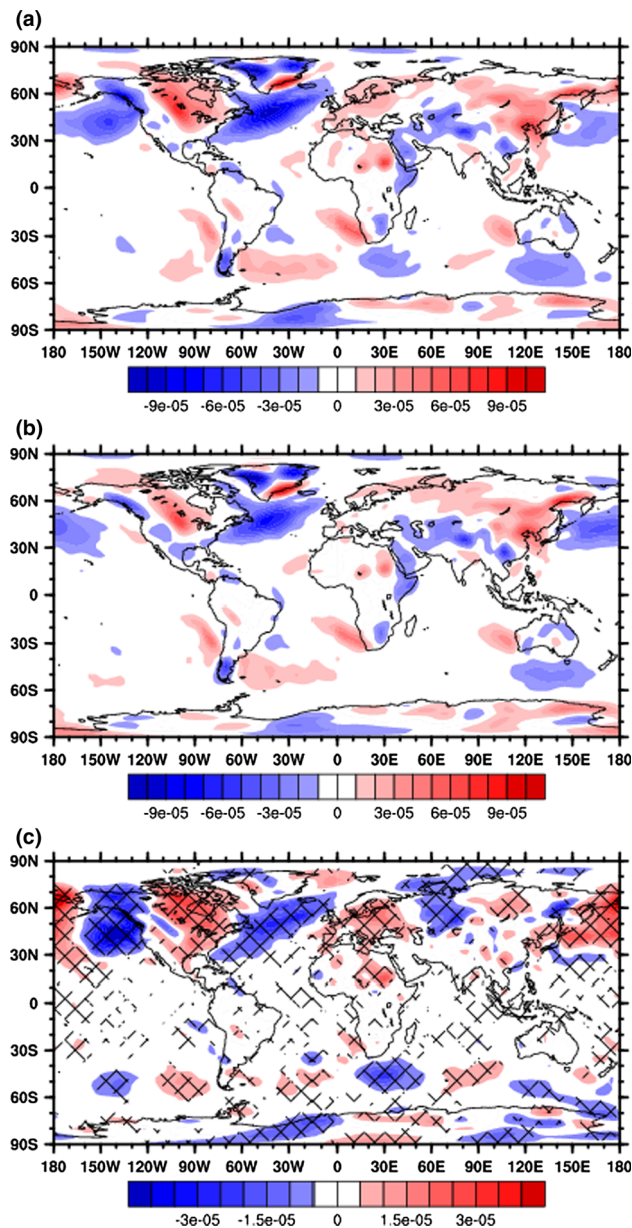


Fig. 9 Composites of the temperature advection at 850 hPa in winter (DJF) for (a) high COWL Index and (b) low COWL Index and (c) the difference between high and low indices (high minus low). The contour intervals are 1.0×10^{-5} k/s in (a) and (b) and 0.5×10^{-5} k/s in (c). The shaded areas in (c) indicate significant values at the 99 % confidence level

7 Discussion and conclusion

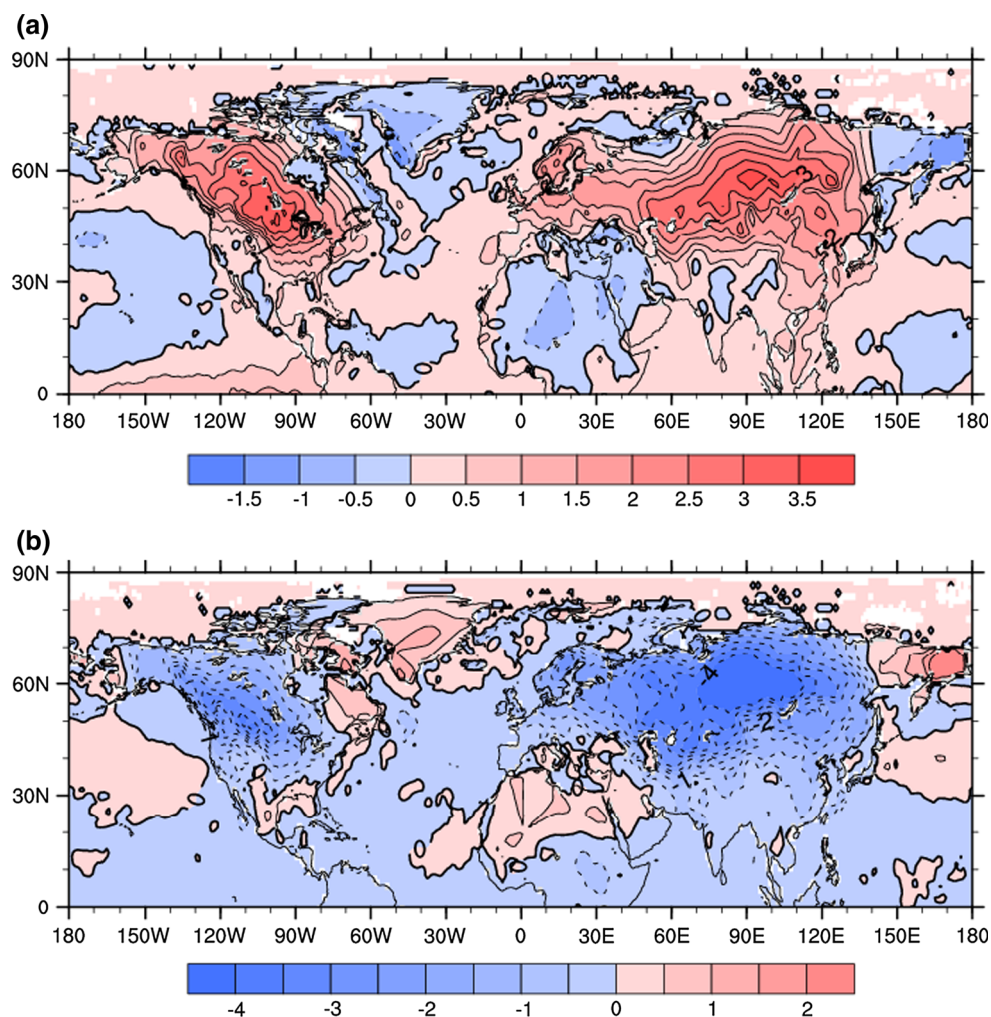
In this study, we investigated the change in the zonal asymmetric thermal forcing associated with the land–sea distribution and the corresponding atmospheric responses during winter. As the continental temperatures have risen more intensely since the mid 1980s, the LSI has moved from a negative to a positive phase. Composite analysis determined that when the LSI was higher, the planetary

waves in the mid-latitudes were weaker due to larger equatorward propagation. Planetary waves exerted a weaker easterly wind forcing on the westerly wind, which caused stronger westerly wind. Thus, a stronger westerly wind would prevail in the positive LSI phase and apparently reduced the meridional heating exchange because of a weaker meridional flow. A strong westerly wind could also advect warm air masses from the oceans to the west of the continents and induce warming in these regions. A similar relationship between zonal wind and temperature advection is also expected to occur on the western side of the continents as a result of annular-mode oscillations (Thompson and Wallace 1998). Much attention was given to the annular-mode variation, but coupled simulations including anthropogenic effects have failed to account for the observed trend in the Northern Annular Mode (NAM). WS04 also demonstrated that the NAM is not sufficient to describe recent interdecadal variation and trends in Northern Hemisphere wintertime circulation. According to WS04, the mid-tropospheric signal was mostly due to the COWL pattern.

Although many studies examined blocking, few explored the statistical and dynamical relationship between blocking and the enhanced warming during cold seasons. By using a simplified model, Charney and DeVore (1979) demonstrated the causal role of the zonally asymmetric thermal forcing in providing a favorable background environment for blocking formation. Results of the composite analysis presented in Sects. 4 and 5 showed that the blocked days were strongly related to the LSI phase in the Atlantic and European regions. We investigated the blocking in terms of its duration and the number of blocking events. During the positive phase, the duration of blocking events was shorter than that during the negative phase. In the Atlantic Ocean, the duration of the negative LSI phase of 11.8 days was 16 % more than that during the positive phase (of 10.1 days). In Europe, the duration of blocking was sensitive to the LSI phase, with blocking events of longer duration being greatly reduced during positive LSI; the number of blocking events persisting for more than 10 days during the positive phase was only half of the number during the negative phase. However, this difference between positive and negative phases was not observed in the Pacific area, which maybe relate with the influence of the Tibetan Plateau; it is possible that another mechanism operates in the region.

In summary, the blocking pattern mainly reflects the superposition of medium-scale waves upon a planetary-scale background that is conducive to blocking formation. For the negative phase of the LSI, the surface thermal forcing followed the “warm ocean/cold land” pattern shown in Fig. 10b, which enhanced the resonance forcing of topography and generated a weakened westerly wind

Fig. 10 Composite surface air temperature anomaly fields in winter (December–February) for positive (a) and negative (b) phase of the LSI. The contour intervals are 0.5 °C



environment that was favorable for the formation and persistence of blocking. As the enhanced warming proceeded in the mid-latitudes in recent decades, the LSI gradually increased and the land–sea thermal contrast was significantly reduced. During the positive phase of the LSI, the surface temperature anomalies followed the distinctive “cold ocean/warm land” pattern shown in Fig. 10a, which reduced the resonance forcing of the topography and acted against the formation and persistence of blocking. The key role of the COWL pattern is the feedback between asymmetric surface thermal forcing (reflected by the LSI) and large-scale circulation. A higher LSI generated weaker planetary wave activity in the mid-latitudes, and a stronger westerly wind or more reduced blocking activity then led to more enhanced continental warming, which would further increase the LSI. Our statistical results linking the reduced blocking to positive LSI were then interpreted using Charney-Devore’s theory. The dynamical connection between the LSI and blocking can be explained as the following. To a large extent, the LSI represents the land–sea temperature

distribution, and at the same time it determines the extent of zonal asymmetric thermal forcing. According to the theoretical model, this asymmetric temperature distribution, in turn, controls the nature of atmospheric circulation. In winter, during the positive phase of the LSI the flow is more zonally orientated and is unfavorable for blocking formation. Blocking events are less frequent, or their lifetimes are much shorter than those during the negative phase of the LSI.

Acknowledgments This work was supported by the National Basic Research Program of China (2012CB955301), the Youth Foundation of China (41305060), the Special Scientific Research Project for Public Interest (GYHY201206009), and the Program for Changjiang Scholars and Innovative Research Team in University. We thank the World Climate Research Program’s Working Group on Coupled Modeling, which is responsible for archiving CMIP outputs, and the climate modeling groups (listed in Table 1 of this paper) for producing and making available their model outputs. For the CMIP the U.S. Department of Energy’s Program for Climate Model Diagnosis and Intercomparison provides coordinating support and leads development of software infrastructure in partnership with the Global Organization for Earth System Science Portals.

Open Access This article is distributed under the terms of the Creative Commons Attribution License which permits any use, distribution, and reproduction in any medium, provided the original author(s) and the source are credited.

References

- Barriopedro D, García-Herrera R, Lupo AR, Hernández E (2006) Climatology of Northern Hemisphere blocking. *J Clim* 19(6):1042–1063
- Charney JG, DeVore JG (1979) Multiple flow equilibria in the atmosphere and blocking. *J Atmos Sci* 36(7):1205–1216
- Chen W, Graf HF, Takahashi M (2002) Observed interannual oscillations of planetary wave forcing in the Northern Hemisphere winter. *Geophys Res Lett* 29(22):2073
- Chen W, Yang S, Huang RH (2005) Relationship between stationary planetary wave activity and the East Asian winter monsoon. *J Geophys Res* 110(D14):D14110
- Cohen JL, Furtado JC, Barlow M, Alexeev VA, Cherry JE (2012) Asymmetric seasonal temperature trends. *Geophys Res Lett* 39(4). doi:10.1029/2011gl050582
- Egger J (1978) Dynamics of blocking highs. *J Atmos Sci* 35:1788–1801
- Favre A, Gershunov A (2006) Extra-tropical cyclonic/anticyclonic activity in North-Eastern Pacific and air temperature extremes in Western North America. *Clim Dyn* 26(6):617–629
- Folland CK, Karl T, Vinnikov K (1990) Observed climate variations and change. *Clim Change IPCC Sci Assess* 195:238
- Gong D, Wang S (1999) Long-term variability of the Siberian high and the possible connection to global warming. *Acta Geogr Sin* 54(2):125–133
- Higuchi K, Huang J, Shabbar A (1999) A wavelet characterization of the North Atlantic oscillation variation and its relationship to the North Atlantic sea surface temperature. *Int J Climatol* 19(10):1119–1129
- Huang J, Higuchi K, Shabbar A (1998) The relationship between the North Atlantic Oscillation and El Niño–Southern Oscillation. *Geophys Res Lett* 25(14):2707–2710
- Huang J, Ji M, Higuchi K, Shabbar A (2006) Temporal structures of the North Atlantic Oscillation and its impact on the regional climate variability. *Adv Atmos Sci* 23(1):23–32. doi:10.1007/s00376-006-0003-8
- Huang J, Guan X, Ji F (2012) Enhanced cold-season warming in semi-arid regions. *Atmos Chem Phys Discuss* 12(2):4627–4653. doi:10.5194/acpd-12-4627-2012
- Huang J, Ji M, Liu Y, Zhang L, Gong D (2013) An overview of arid and semi-arid climate change. *Adv Clim Change Res* 9(1):9–14
- Hudgins L, Huang J (1996) Bivariate wavelet analysis of Asia monsoon and ENSO. *Adv Atmos Sci* 13(3):299–312
- Ji M, Huang J, Wang S, Wang X, Zheng Z, Ge J (2008) Winter blocking episodes and impact on climate over East Asia. *Plateau Meteorol* 02:415–421
- Jones P, Briffa K (1992) Global surface air temperature variations during the twentieth century: part 1, spatial, temporal and seasonal details. *The Holocene* 2(2):165–179
- Kaas E, Branstator G (1993) The relationship between a zonal index and blocking activity. *J Atmos Sci USA* 50(18):3061–3077
- Kalnay E, Kanamitsu M, Kistler R, Collins W, Deaven D, Gandin L, Iredell M, Saha S, White G, Woollen J (1996) The NCEP/NCAR 40-year reanalysis project. *Bull Am Meteorol Soc* 77(3):437–471
- Kucharski F, Molteni F, Bracco A (2005) Decadal interactions between the western tropical Pacific and the North Atlantic Oscillation. *Clim Dyn* 26(1):79–91. doi:10.1007/s00382-005-0085-5
- Kung EC, Dacamura CC, Baker WE, Susskind J, Park CK (1990) Simulations of winter blocking episodes using observed sea surface temperatures. *Q J R Meteorol Soc* 116(495):1053–1070
- Li J, Wang JXL (2003) A modified zonal index and its physical sense. *Geophys Res Lett* 30(12):1632
- Limpasuvan V, Hartmann DL (1999) Eddies and the annular modes of climate variability. *Geophys Res Lett* 26(20):3133–3136
- Luo D (2005) Why is the North Atlantic block more frequent and long-lived during the negative NAO phase? *Geophys Res Lett* 32(20). doi:10.1029/2005gl022927
- Manabe S, Stouffer RJ (1980) Sensitivity of a global climate model to an increase of CO₂ concentration in the atmosphere. *J Geophys Res* 85(C10):5529–5554
- Mitchell TD, Jones PD (2005) An improved method of constructing a database of monthly climate observations and associated high-resolution grids. *Int J Climatol* 25(6):693–712
- Molteni F, King MP, Kucharski F, Straus DM (2011) Planetary-scale variability in the northern winter and the impact of land–sea thermal contrast. *Clim Dyn* 37(1):151–170
- Panagiotopoulos F, Shahgedanova M, Hannachi A, Stephenson DB (2005) Observed trends and teleconnections of the Siberian high: a recently declining center of action. *J Clim* 18(9):1411–1422
- Rayner N, Parker D, Horton E, Folland C, Alexander L, Rowell D, Kent E, Kaplan A (2003) Global analyses of sea surface temperature, sea ice, and night marine air temperature since the late nineteenth century. *J Geophys Res* 108(D14):4407
- Robock A (1983) Ice and snow feedbacks and the latitudinal and seasonal distribution of climate sensitivity. *J Atmos Sci* 40(4):986–997
- Shabbar A, Huang J, Higuchi K (2001) The relationship between the wintertime north Atlantic oscillation and blocking episodes in the north Atlantic. *Int J Climatol* 21(3):355–369. doi:10.1002/joc.612
- Taylor KE, Stouffer RJ, Meehl GA (2012) An overview of CMIP5 and the experiment design. *Bull Am Meteorol Soc* 93(4):485–498
- Thompson DWJ, Wallace JM (1998) The Arctic oscillation signature in the wintertime geopotential height and temperature fields. *Geophys Res Lett* 25(9):1297. doi:10.1029/98gl00950
- Tibaldi S, Molteni F (1990) On the operational predictability of blocking. *Tellus A* 42(3):343–365
- Tung K, Lindzen R (1979) A theory of stationary long waves, part I: a simple theory of blocking. *Mon Wea Rev* 107(6):714–734
- Wallace JM, Zhang Y, Bajuk L (1996) Interpretation of interdecadal trends in Northern Hemisphere surface air temperature. *J Clim* 9(2):249–259
- Wang L, Chen W, Zhou W, Huang R (2009) Interannual variations of East Asian trough axis at 500 hPa and its association with the East Asian winter monsoon pathway. *J Clim* 22(3):600–614
- Wang L, Chen W, Zhou W, Chan JC, Barriopedro D, Huang R (2010) Effect of the climate shift around mid 1970s on the relationship between wintertime Ural blocking circulation and East Asian climate. *Int J Climatol* 30(1):153–158
- Wu Q, Straus DM (2004) AO, COWL, and observed climate trends. *J Clim* 17(11):2139–2156